Journal of The Electrochemical Society

OPEN ACCESS

Raman Analysis and Electrochemical Reduction of Silicate Ions in Molten NaCl–$CaCl_2$

To cite this article: Yuanjia Ma *et al* 2021 *J. Electrochem. Soc.* **168** 046515

Journal of The Electrochemical Society, 2021 **168** 046515

Raman Analysis and Electrochemical Reduction of Silicate Ions in Molten NaCl–$CaCl_2$

Yuanjia Ma,[1] Takayuki Yamamoto,[1] Kouji Yasuda,[2,3,a] and Toshiyuki Nohira[1,z]

[1]*Institute of Advanced Energy, Kyoto University, Gokasho, Uji, Kyoto 611-0011, Japan*
[2]*Graduate School of Energy Science, Kyoto University, Yoshida-honmachi, Sakyo-ku, Kyoto 606-8501, Japan*
[3]*Agency for Health, Safety and Environment, Kyoto University, Yoshida-honmachi, Sakyo-ku, Kyoto 606-8501, Japan*

This study investigated the ionic species and electrochemical reduction of silicate ions at a solid graphite electrode in molten NaCl–$CaCl_2$ eutectic melts with various concentrations of O^{2-} ion at 1023 K. Silicate ion species in the melts with various O^{2-}/SiO_2 ratios (r_{O^{2-}/SiO_2}) were determined by Raman spectroscopy. The dominant species was SiO_3^{2-} for $r_{O^{2-}/SiO_2} = 1.0$, and SiO_4^{4-} for $r_{O^{2-}/SiO_2} = 1.5$ and 2.0. From cyclic voltammetry, XRD, and SEM analyses, electrochemical reduction was indicated for SiO_3^{2-} and SiO_4^{4-} at more negative than 1.0 V and 0.80 V vs Na^+/Na, respectively. Formation of $CaSi_2$ was confirmed at 0.50 V in all molten salts with $r_{O^{2-}/SiO_2} = 1.0$, 1.5, and 2.0. The potential ranges for pure Si deposition are almost the same in molten salts with $r_{O^{2-}/SiO_2} = 1.0$ and 1.5.
 [DOI: 10.1149/1945-7111/abf4b2]

Manuscript submitted January 12, 2021; revised manuscript received March 16, 2021. Published April 22, 2021. *This was paper 3000 presented during PRiME 2020, October 4–9, 2020.*

Photovoltaic (PV) power generation is considered a source of clean and inexhaustible energy, which could be a substitute for conventional fossil-fuel power generation. According to the World Energy Outlook 2018 by the International Energy Agency (IEA), the share of PV power in the worldwide energy supply is expected to increase from 1.7% in 2017[1,2] to 10% by 2040 if the cost of PV cell production is reduced. The global production of PV cells reached 102.4 GW in 2018, approximately 350 times the value in 2000.[3] Since crystalline Si solar cells account for 96.9% of the worldwide production in 2018,[4] they are expected to remain mainstream in the PV industry for the time being. Thus, the global demand for high-purity crystalline Si, which is known as solar-grade Si (SOG-Si), will continue to increase in the future.

Currently, approximately 90% of SOG-Si is produced using the Siemens process.[5–8] Although the purity of Si produced in the Siemens process is sufficiently high, low productivity and high energy consumption hinder cost reduction. To develop a next-generation production process for SOG-Si, experimental studies on the purification of metallurgical-grade Si[9–13] and metallothermic reduction of silicon halides by metal reductants[14–17] have been conducted.

Over the past two decades, we have been studying the electrochemical reduction of solid SiO_2 to Si in molten $CaCl_2$ as a new production process for SOG-Si.[18–31] In molten $CaCl_2$, the electrochemical reduction of insulating SiO_2 proceeds by using a SiO_2 contacting electrode, which provides a three-phase interface of conductor/SiO_2/$CaCl_2$.

$$SiO_2(s) + 4e^- \rightarrow Si(s) + 2O^{2-} \quad [1]$$

To achieve efficient recovery of reduced Si, we proposed an electrochemical reduction process of SiO_2 using a liquid Zn cathode in molten $CaCl_2$.[32–34] The overall process consists of three major steps: electrolysis, precipitation, and refining. In the electrolysis step, the solid SiO_2 is reduced to form a Si–Zn liquid alloy. Then, solid Si is precipitated by lowering the temperature of the liquid Si–Zn alloy during the precipitation step. The recovered Si is subjected to a refining step that comprises vacuum refining to remove residual Zn and directional solidification to manufacture SOG-Si ingots.

In our previous study, we found that the direct electrochemical reduction of solid SiO_2 mainly occurred at the three-phase interface of Zn/SiO_2/$CaCl_2$. In addition to this, the liquid Ca–Zn alloy, which forms at potentials more negative than 0.60 V (vs Ca^{2+}/Ca), contributed to the indirect reduction of SiO_2 below the Zn/$CaCl_2$ interface, that is, in the liquid Zn cathode. In such cases, however, the current efficiency was low because only a part of the Ca–Zn alloy contributed to the reduction of SiO_2.[34]

To improve the productivity of the process, we focused on the electrochemical reduction of dissolved SiO_2, that is, silicate ions (such as SiO_4^{4-}, SiO_3^{2-}, and $Si_2O_5^{2-}$). When O^{2-} ion is added to the molten salt, the dissolution of SiO_2 can be expressed as follows:

$$xSiO_2(s) + yO^{2-} \rightarrow Si_xO_{(2x+y)}^{2y-} \quad [2]$$

The electrodeposition of crystalline Si films from silicate ions at a solid substrate in molten $CaCl_2$ has been reported by Bard and co-workers.[35–37] However, the ionic species of silicates has not yet been investigated.

In this study, we used eutectic NaCl–$CaCl_2$, which has a lower melting point (777 K) than that of pure $CaCl_2$ (1045 K). The ionic species of silicates in molten eutectic NaCl–$CaCl_2$ with various concentrations of CaO was investigated by Raman spectroscopy. Since the concentration of CaO used in this study is lower than its solubility (7.6 mol%),[38] it is considered to be completely dissociated into Ca^{2+} and O^{2-}. Then, the electrochemical reduction of silicate ions was investigated at a solid graphite substrate as a preliminary study for a liquid Zn cathode.

Experimental

All of the experiments were conducted in a dry Ar atmosphere at 1023 K. The experimental procedures for (a) Raman spectroscopy and (b) electrochemical reduction of silicate ions are described as follows.

Raman spectroscopy of silicate ions.—Salt preparation was conducted in a dry Ar-filled glove box (less than 1 ppm O_2 and 1 ppm H_2O). NaCl and $CaCl_2$ powders (FUJIFILM Wako Pure Chemical Corp., reagent grade) were mixed in a eutectic composition (NaCl:$CaCl_2$ = 47.9:52.1 mol%). Pre-determined amounts of CaO (FUJIFILM Wako Pure Chemical Corp., 98.0%), SiO_2 (Sigma-Aldrich, 10–20 nm, 99.5%), and $CaSiO_3$ (Sigma-Aldrich, 200 mesh, 99%) powders were added to the eutectic mixture. CaO was dried at

[a]Present address: Graduate School of Engineering, Kyoto University, Kyoto 606–8501, Japan.
[z]E-mail: nohira.toshiyuki.8r@kyoto-u.ac.jp

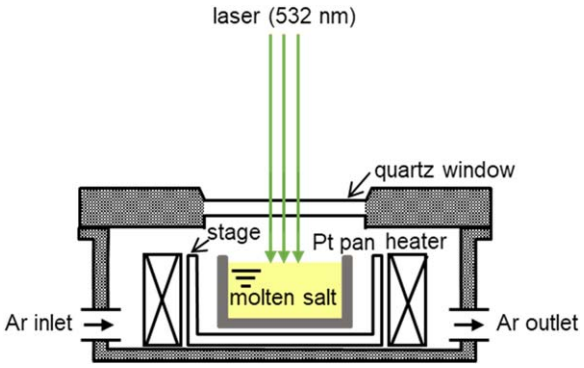

Figure 1. Schematic of experimental apparatus for Raman spectroscopy of molten salt.

1273 K for 2 h. SiO_2 and $CaSiO_3$ were added as received. The added amounts were 0, 0.5, and 1.0 mol% for CaO, 0 and 1.0 mol% for SiO_2, and 0 and 1.0 mol% for $CaSiO_3$. The mixture was loaded into a graphite crucible (Toyo Tanso Co., Ltd, IG-110 grade, o.d. 55 mm × i.d. 49 mm × height 150 mm) and dried under vacuum at 453 K for 2 d and then at 723 K for 1 d. After the temperature was increased to 1023 K and maintained for 1 d to sufficiently dissolve the additives, the salt was quickly sampled using a borosilicate glass tube (Pyrex®, o.d. 6 mm × i.d. 4 mm).

Figure 1 shows a schematic drawing of the experimental apparatus used for Raman spectroscopy. The sampled salt was then loaded into a Pt pan (Rigaku Corp., o.d. 5 mm × height 2.5 mm) and placed in an airtight high-temperature stage (Japan High Tech Co., Ltd, 10042). After the mixture was heated to 1023 K, the ionic species of silicates was investigated using a micro-Raman spectrometer (Tokyo Instruments, Nanofinder 30) using a laser source with an excitation wavelength of 532 nm. Origin 2020 software was used to deconvolve the spectra using the Viogtian function.

Electrochemical reduction of silicate ions.—NaCl and $CaCl_2$ powders were mixed in the eutectic composition and loaded into a graphite crucible (Toyo Tanso Co., Ltd, IG-110 grade, o.d. 100 mm × i.d. 95 mm × height 120 mm). The crucible was placed at the bottom of a graphite vessel in an airtight Kanthal container. The eutectic mixture was dried under vacuum at 453 K for 2 d and at 723 K for 1 d. After the temperature was raised to 1023 K, predetermined amounts of CaO (0, 0.5 or 1.0 mol%) and $CaSiO_3$ (1.0 mol%) powders were added to the eutectic mixture.

Figure 2 shows a schematic drawing of the experimental apparatus for the electrochemical reduction of silicate ions. All electrochemical measurements were conducted by a three-electrode method using an electrochemical measurement system (Hokuto Denko Corp., HZ-7000) in a glove box. As the working electrodes, a flag-shaped graphite plate (Toyo Tanso Co., Ltd, 3 mm × 3 mm × thickness 0.5 mm) was used for cyclic voltammetry and a graphite plate (Toyo Tanso Co., Ltd, 10 mm × 10 mm × thickness 0.5 mm) was used for electrolysis. The counter electrodes were glass-like carbon (Tokai Carbon Co., Ltd, diameter: 3.0 mm) for cyclic voltammetry and a graphite square bar (Toyo Tanso Co., Ltd, 5 mm × 5 mm) for electrolysis. A Si square bar (Furuuchi Chemical Corp., 5 mm × 5 mm, 10 N purity) was used as the quasi-reference electrode. The potential of the reference electrode was calibrated with respect to a dynamic Na^+/Na potential, determined by cyclic voltammetry on a Mo wire (Nilaco Corp., diameter 1.0 mm) electrode.

The obtained samples were washed in an 1 M HCl solution prepared from FUJIFILM Wako Pure Chemical Corp., reagent grade, 36 wt.% at 333 K for 15 min to remove the salt adhered to the deposits. The surfaces of the samples were observed using an optical microscope (Thanko Inc., DILITE30) and scanning electron microscope (SEM, Thermo Fisher Scientific Inc., Phenom Pro

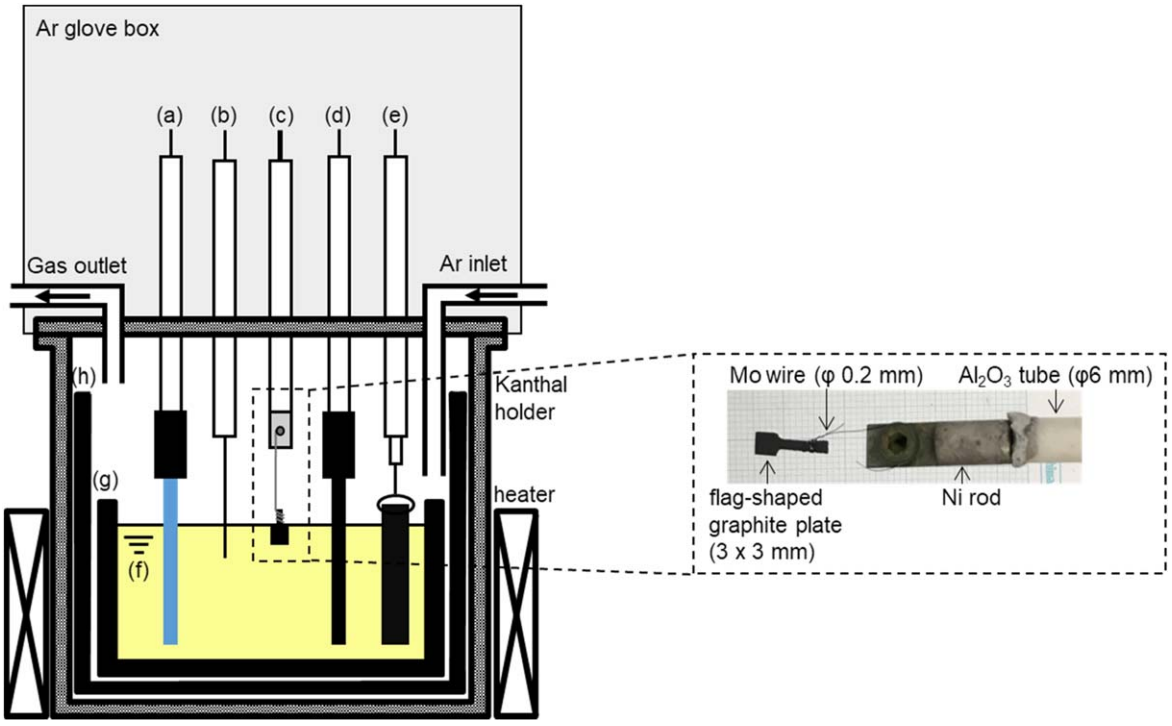

Figure 2. Schematic of the electrolysis cell. (a) Si quasi-reference electrode, (b) Na^+/Na dynamic reference electrode on a Mo wire, (c) flag-like graphite working electrode, (d) glass-like carbon counter electrode, (e) graphite counter electrode, (f) molten NaCl–$CaCl_2$ containing CaO and $CaSiO_3$, (g) graphite crucible, and (h) graphite holder.

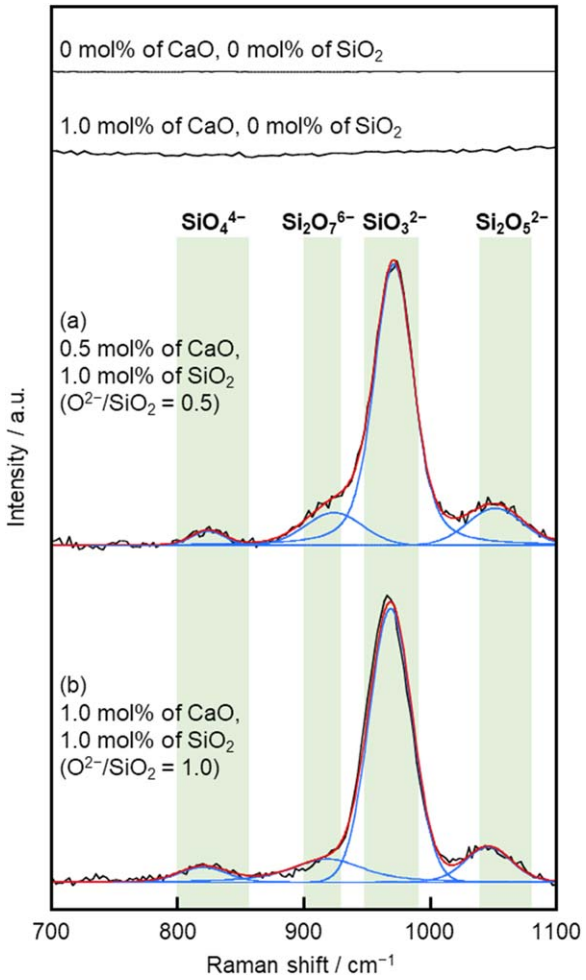

Figure 3. Original and deconvolved Raman spectra for molten eutectic NaCl–$CaCl_2$ containing different amounts of CaO and SiO_2 at 1023 K.

Generation 5). The deposits were also characterized by X-ray diffraction (XRD, Rigaku, Ultima IV, Cu-Kα, λ = 1.5418 Å, 40 kV, 40 mA).

Result and Discussion

Ionic species of silicates.—Figure 3 shows original and deconvolved Raman spectra for molten eutectic NaCl–$CaCl_2$ containing different amounts of CaO and SiO_2 at 1023 K. The original spectra were shown with background subtracted. Within the wavenumber range of 700–1100 cm^{-1}, no bands were observed for the melts without SiO_2. For the melts containing 0.5 mol% CaO and 1.0 mol% SiO_2 ($r_{O^{2-}/SiO_2} = 0.5$), and that with addition of 1.0 mol% CaO and 1.0 mol% SiO_2 ($r_{O^{2-}/SiO_2} = 1.0$), a strong band was detected near 970 cm^{-1} and several weak bands at about 820, 920, and 1050 cm^{-1}.

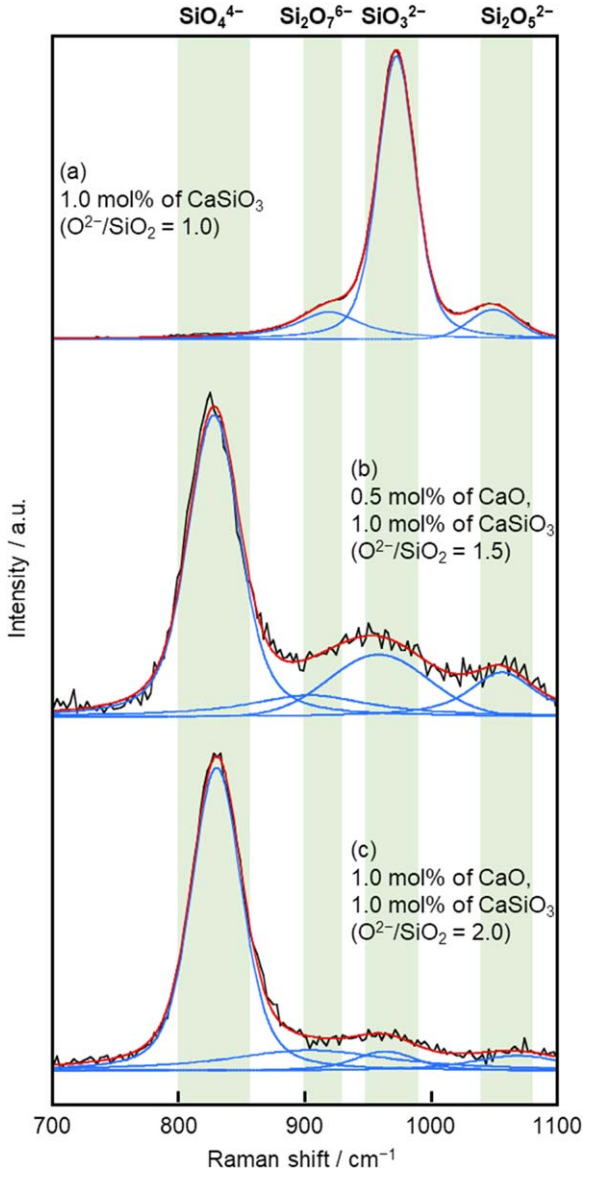

Figure 4. Original and deconvolved Raman spectra for molten NaCl–$CaCl_2$ containing different amounts of CaO and $CaSiO_3$.

Table I. Raman spectroscopy data for samples that obtained in molten NaCl–$CaCl_2$ containing different amounts of CaO and $CaSiO_3$.

Melt composition	Wavenumber / cm^{-1} (Band intensity fraction† / %)			
	SiO_4^{4-}	$Si_2O_7^{6-}$	SiO_3^{2-}	$Si_2O_5^{2-}$
1.0 mol% of $CaSiO_3$ (O^{2-}/SiO_2 = 1.0)	—	920w (15.6)	974 s (75.9)	1050vw (8.6)
0.5 mol% of CaO, 1.0 mol% of $CaSiO_3$ (O^{2-}/SiO_2 = 1.5)	829 s (57.0)	905w (11.9)	960w (18.7)	1058w (12.5)
1.0 mol% of CaO, 1.0 mol% of $CaSiO_3$ (O^{2-}/SiO_2 = 2.0)	831 s (67.9)	905w (18.7)	965vw (5.8)	1070vw (7.6)

Abbreviations: vw, very weak; w, weak; s, strong. †) Calculated from fitted band area.

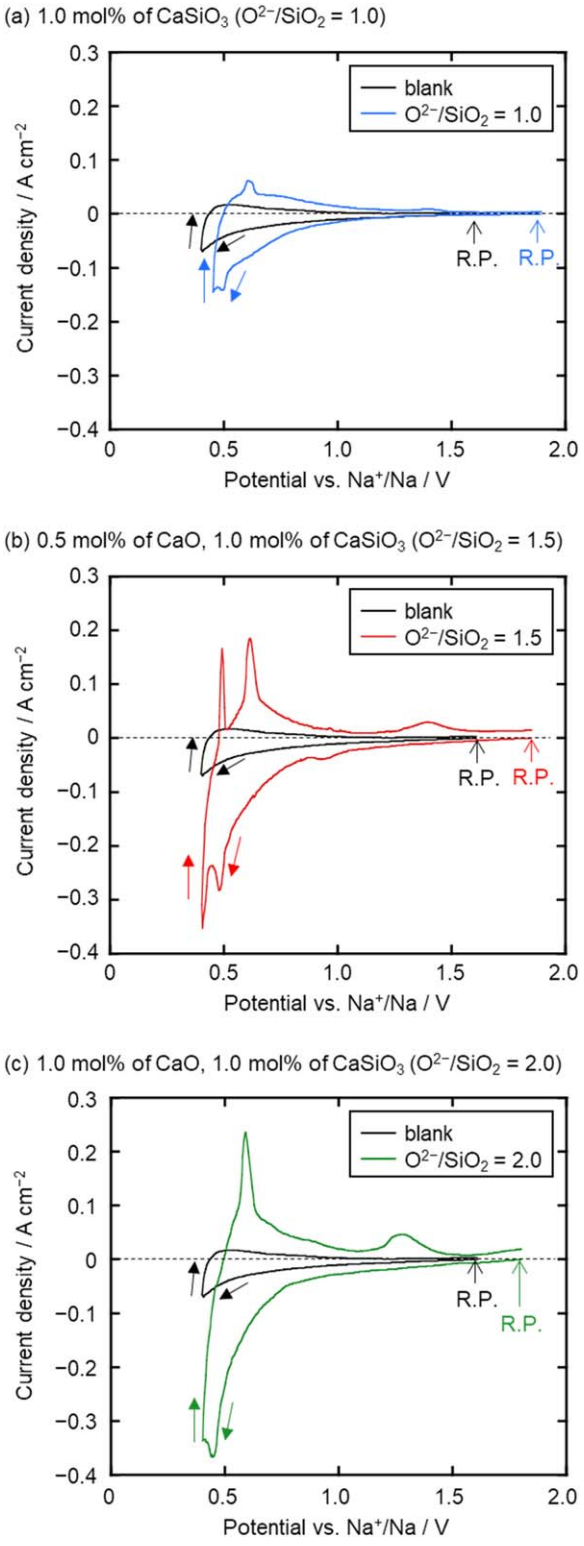

Figure 5. Cyclic voltammograms at a graphite electrode in molten NaCl–$CaCl_2$ before and after the addition of (a) 1.0 mol% of $CaSiO_3$, (b) 0.5 mol% of CaO and 1.0 mol% of $CaSiO_3$, and (c) 1.0 mol% of CaO and 1.0 mol% of $CaSiO_3$ at 1023 K. Scan rate: 50 mV s^{-1}. R. P.: Rest potential.

The spectra were deconvolved using the Voigtian function. According to previous studies,[39–41] the symmetric stretch vibrations of SiO_4^{4-}, $Si_2O_7^{6-}$, SiO_3^{2-} and $Si_2O_5^{2-}$ are reported at 850–880, 900–920, 950–980, and 1050–1100 cm^{-1}, respectively. Therefore, bands at 920, 972 and 1053 cm^{-1} are assigned to $Si_2O_7^{6-}$, SiO_3^{2-} and $Si_2O_5^{2-}$. The band at 825 cm^{-1} in our data could be attributed to SiO_4^{4-} vibration. However, the wavenumber is slightly lower than the reported value, 850–880 cm^{-1}, for SiO_4^{4-}. Wang et al. reported that the Raman spectra for CaO–SiO_2–$CaCl_2$ slags gradually shift to lower wavenumber with increasing chlorine content, and that chlorine atoms can also be substituted with oxygen atoms.[42] Thus, oxygen atoms of SiO_4^{4-} ion might be partially substituted with chlorine atoms according to the following reaction.

$$SiO_4^{4-} + Cl^- \rightarrow SiO_3Cl^{3-} + O^{2-} \quad [3]$$

Similar fitting results were obtained for the melt with $r_{O^{2-}/SiO_2} = 1.0$; there is a strong band at 968 cm^{-1} for SiO_3^{2-}, and three weak bands at 822, 920, and 1050 cm^{-1} attributed to SiO_4^{4-}, $Si_2O_7^{6-}$, and $Si_2O_5^{2-}$, respectively. As the dominant silicate ion was SiO_3^{2-} in the melts with $r_{O^{2-}/SiO_2} \leqslant 1.0$, the dissolution limit of SiO_2 is likely to be determined by the O^{2-} content. In addition, the weak bands of SiO_4^{4-}, $Si_2O_7^{6-}$, and $Si_2O_5^{2-}$ were observed because of the equilibrium reactions of SiO_3^{2-} and $Si_2O_7^{6-}$.

$$4SiO_3^{2-} \rightleftarrows Si_2O_7^{6-} + Si_2O_5^{2-} \quad [4]$$

$$Si_2O_7^{6-} \rightleftarrows SiO_4^{4-} + SiO_3^{2-} \quad [5]$$

As mentioned above, the ionic species of SiO_2 in melts with $r_{O^{2-}/SiO_2} \leqslant 1.0$ was mainly attributed to SiO_3^{2-}. To further investigate the stable silicate ions in the melts with various r_{O^{2-}/SiO_2} values ($\geqslant 1.0$), $CaSiO_3$ was used as the SiO_2 source. This is because the dissolution rate of $CaSiO_3$ is significantly higher than that of SiO_2, which enables the quick preparation of the melts with target compositions. By adding CaO as the O^{2-} source, melts with $r_{O^{2-}/SiO_2} = 1.0$, 1.5, and 2.0 were prepared and analyzed by Raman spectroscopy. Figure 4 shows the original and deconvolved Raman spectra of the melts. Figure 4(a) was deconvolved to 3 bands at 920 cm^{-1} for $Si_2O_7^{6-}$, 972 cm^{-1} for SiO_3^{2-}, and 1050 cm^{-1} for $Si_2O_5^{2-}$. For the deconvolution of Fig. 4(b), the band near 830 cm^{-1} was added and the spectra were deconvolved to 4 bands. Although the band for $Si_2O_7^{6-}$ is weak, the coefficient of determination, R^2, for 4 bands is 0.9909, which is higher than that for 3 bands without $Si_2O_7^{6-}$ band ($R^2 = 0.9842$). Therefore, Figs. 4b and 4c were deconvolved to 4 bands. The deconvolution results of the Raman spectra are presented in Table I. As the result, for the melt with $r_{O^{2-}/SiO_2} = 1.0$, the dominant silicate ion is SiO_3^{2-}, which is consistent with the melt with the same r_{O^{2-}/SiO_2} prepared from CaO and SiO_2. When r_{O^{2-}/SiO_2} increased to 1.5, the dominant silicate species was SiO_4^{4-}, secondary dominant SiO_3^{2-}, and minor $Si_2O_7^{6-}$ and $Si_2O_5^{2-}$. Although the ratio of $O^{2-}/SiO_2 = 1.5$ corresponds to $Si_2O_7^{6-}$ ion, the equilibrium reaction of $Si_2O_7^{6-}$ (reaction 5) would occur because of its poor stability in the melt. With respect to the melt with $r_{O^{2-}/SiO_2} = 2.0$, SiO_4^{4-} is the dominant silicate ion which is consistent with the composition calculated from the O^{2-}/SiO_2 ratio.

Electrochemical reduction of silicate ions.—Figure 5 shows the cyclic voltammograms of a graphite electrode in molten NaCl–$CaCl_2$ containing different amounts of CaO and $CaSiO_3$. The black curves show the voltammograms before the addition of $CaSiO_3$ and CaO (blank). The small cathodic current observed around 0.5 V (vs Na^+/Na) is likely due to the intercalation of Ca^{2+} into graphite. After the addition of 1.0 mol% $CaSiO_3$ ($r_{O^{2-}/SiO_2} = 1.0$), as shown in Fig. 5a, cathodic currents increased from 1.0 V, suggesting the electrochemical reduction of dominant SiO_3^{2-} that observed in the Raman data (Fig. 4a). A larger cathodic current peak at around 0.50 V is considered as the formation of Na–Si and/or Ca–Si alloys. Figure 5b shows the voltammogram measured after the addition of 0.50 mol% CaO and 1.0 mol% $CaSiO_3$ ($r_{O^{2-}/SiO_2} = 1.5$). A small cathodic peak observed at 0.95 V is likely due to the electrochemical reduction of secondary dominant SiO_3^{2-} that observed in the Raman data (Fig. 4b). Cathodic currents increased

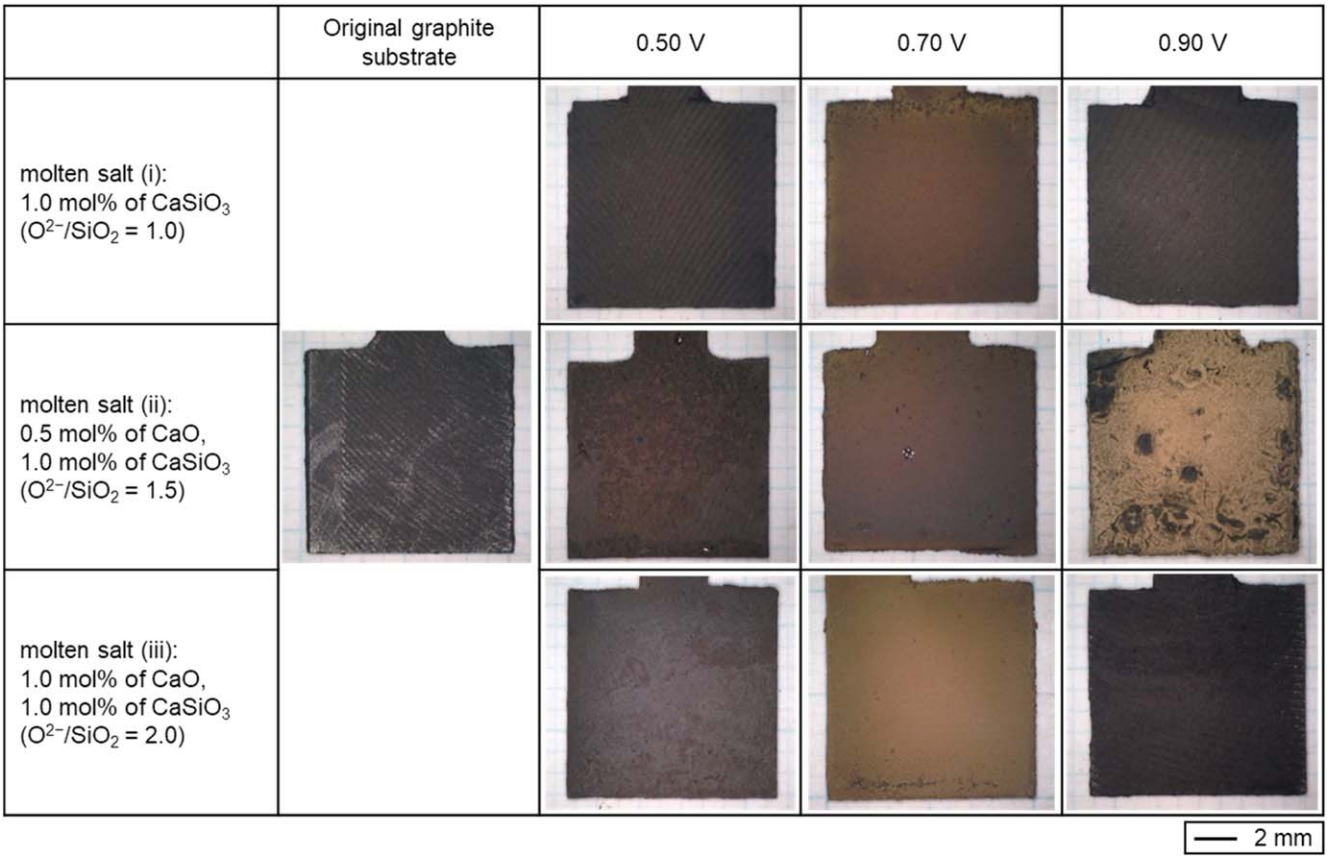

Figure 6. Optical images of a graphite substrate and the samples obtained by electrolysis (0.50 V, 0.70 V, and 0.90 V) at graphite plates in molten NaCl–$CaCl_2$ containing different amounts of CaO and $CaSiO_3$ (left vertical colum) at 1023 K. Charge density: -14 C cm^{-2}.

rapidly from 0.80 V, which seems to be due to the electrochemical reduction of dominant SiO_4^{4-}. The larger currents compared to Fig. 5a suggest that diffusion coefficient of SiO_4^{4-} is larger than that of SiO_3^{2-}. Since SiO_4^{4-} ions are known to have weaker interaction each other compared with SiO_3^{2-} ions,[39] it is reasonable that the effective size of SiO_4^{4-} is smaller than that of SiO_3^{2-}. A cathodic current peak at around 0.50 V is regarded as the formation of Na–Si and/or Ca–Si alloys, which is similar to that observed in Fig. 5a. A voltammogram of the melt containing 1.0 mol% CaO and 1.0 mol% $CaSiO_3$ ($r_{O^{2-}/SiO_2} = 2.0$) is shown in Fig. 5c. A rapid increase of cathodic current from 0.75 V is likely attributed to the electrochemical reduction of dominant SiO_4^{4-}. The current peak at around 0.50 V is ascribed to the same reaction of Na–Si and/or Ca–Si alloys formation, similar to the other two melts in Figs. 5a and 5b.

Based on the voltammetry results, potentiostatic electrolysis was conducted at 0.50, 0.70, and 0.90 V with a constant charge density of -14 C cm^{-2} in molten NaCl–$CaCl_2$ containing (i) 1.0 mol% $CaSiO_3$ ($r_{O^{2-}/SiO_2} = 1.0$), (ii) 0.5 mol% CaO and 1.0 mol% $CaSiO_3$ ($r_{O^{2-}/SiO_2} = 1.5$), and (iii) 1.0 mol% CaO and 1.0 mol% $CaSiO_3$ ($r_{O^{2-}/SiO_2} = 2.0$). Optical images of the original graphite substrate and electrolyzed samples are shown in Fig. 6. Deposits in brown or dark brown color were observed at all samples except the sample obtained at 0.90 V in molten salt (iii). No significant deposits were observed at that sample.

Figure 7 shows XRD patterns of an original graphite substrate and the electrolyzed samples. In Fig. 7a, the existence of Si was confirmed in the samples obtained at 0.70 V and 0.90 V in molten salt (i). Thus, the increase in cathodic current from 1.0 V in Fig. 5a is confirmed to be the electrochemical reduction of SiO_3^{2-} to solid Si.

$$SiO_3^{2-} + 4e^- \rightarrow Si(s) + 3O^{2-} \quad [6]$$

The XRD pattern at 0.50 V indicated the existence of $CaSi_2$, which was identified by the strongest peak at 32.0 degree (relative intensity 100), and the second-strongest one at 46.8 degree (relative intensity 42). Since $CaSi_2$ was identified at 0.50 V, the cathodic current peak at 0.50 V corresponds to the formation of $CaSi_2$.

$$2Si(s) + Ca^{2+} + 2e^- \rightarrow CaSi_2(s) \quad [7]$$

$$2SiO_3^{2-} + Ca^{2+} + 10e^- \rightarrow CaSi_2(s) + 6O^{2-} \quad [8]$$

In molten salt (ii), only Si deposits were confirmed for samples obtained at 0.70 and 0.90 V. As approximately 20% of SiO_3^{2-} was confirmed by Raman spectroscopy, as shown in Table I, the small cathodic peak at 0.95 V is considered to be the electrochemical reduction of SiO_3^{2-} to solid Si (reaction 6). The cathodic current increase from 0.80 V is attributed to the electrochemical reduction of SiO_4^{4-}.

$$SiO_4^{4-} + 4e^- \rightarrow Si(s) + 4O^{2-} \quad [9]$$

In order to confirm the results shown above, thermodynamic data associated with the electrochemical reduction of SiO_3^{2-} and SiO_4^{4-} were calculated. Generally, the difference in reduction potential of SiO_3^{2-} and SiO_4^{4-} can be calculated from the Gibbs energies for the decomposition reactions, $\Delta G_d(l, \text{in melt})$.

$$CaSiO_3(l, \text{in melt}) \rightarrow Si(s) + CaO(l) + O_2(g) \quad [10]$$

$$Ca_2SiO_4(l, \text{in melt}) \rightarrow Si(s) + 2CaO(l) + O_2(g) \quad [11]$$

Here, $CaSiO_3(l, \text{in melt})$ and $Ca_2SiO_4(l, \text{in melt})$ are $CaSiO_3$ and $Ca2SiO_4$ dissolved into molten salt. However, these Gibbs energies

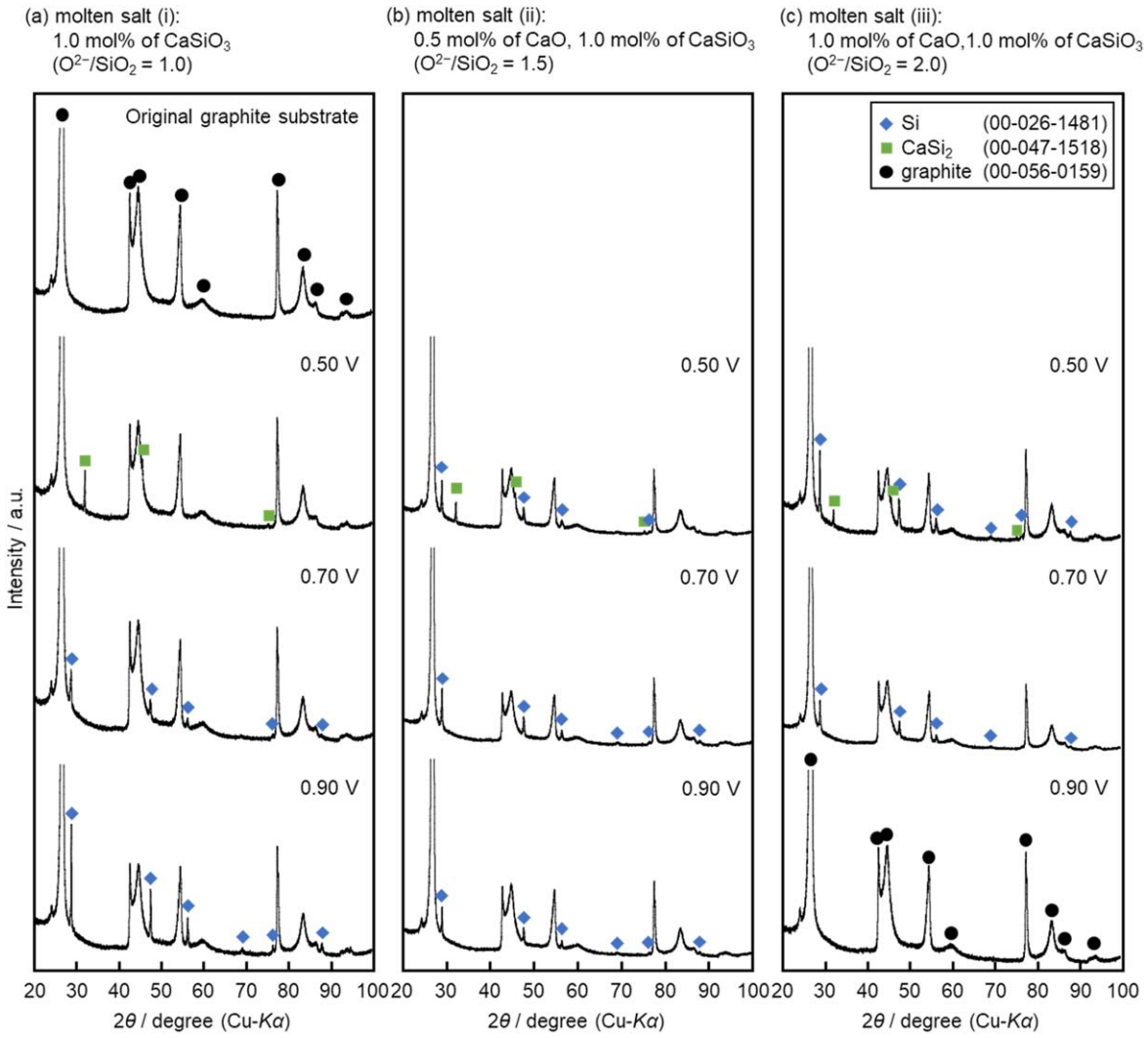

Figure 7. XRD patterns of a graphite substrate and the samples obtained by electrolysis at graphite plates in molten NaCl–$CaCl_2$ containing different amounts of CaO and $CaSiO_3$ at 1023 K. Charge density: -14 C cm^{-2}.

Table II. XRD results for samples in molten NaCl–$CaCl_2$ containing different amounts of CaO and $CaSiO_3$.

Melt composition	Identified phase of electrolyzed samples		
	0.50 V	0.70 V	0.90 V
1.0 mol% of $CaSiO_3$ ($O^{2-}/SiO_2 = 1.0$)	$CaSi_2$	Si	Si
0.5 mol% of CaO, 1.0 mol% of $CaSiO_3$ ($O^{2-}/SiO_2 = 1.5$)	Si $CaSi_2$	Si	Si
1.0 mol% of CaO, 1.0 mol% of $CaSiO_3$ ($O^{2-}/SiO_2 = 2.0$)	Si $CaSi_2$	Si	no deposit

can not be calculated from the reported data. On the other hand, the Gibbs energies for the decomposition reactions for solid $CaSiO_3$ and Ca_2SiO_4, $\Delta G_d(s)$, can be calculated from literature.[43,44]

$$CaSiO_3(s) \rightarrow Si(s) + CaO(l) + O_2(g) \quad [12]$$

$$Ca_2SiO_4(s) \rightarrow Si(s) + 2CaO(l) + O_2(g) \quad [13]$$

Here, we assumed that the difference of the Gibbs energy, $\Delta G_d(l$, in melt$) - \Delta G_d(s)$, is almost same for $CaSiO_3$ and Ca_2SiO_4, so that $\Delta G_d(s)$ could be used to estimate the difference in reduction potential of SiO_3^{2-} and SiO_4^{4-}. The calculated data are shown in Table III. Since the standard Gibbs energy for $CaSiO_3(s)$ is smaller than that for $Ca_2SiO_4(s)$, the electrochemical reduction of SiO_3^{2-} would start from a more positive potential than SiO_4^{4-}. From the

Table III. Standard Gibbs energies for decomposition reactions of $CaSiO_3(s)$ and $Ca_2SiO_4(s)$ to Si(s), CaO(l), and $O_2(g)$ at 1023 K.

Reaction	Standard Gibbs energy, ΔG° / kJ mol^{-1}
$CaSiO_3(s) \rightarrow Si(s) + CaO(l) + O_2(g)$	869.4
$Ca_2SiO_4(s) \rightarrow Si(s) + 2\,CaO(l) + O_2(g)$	970.0

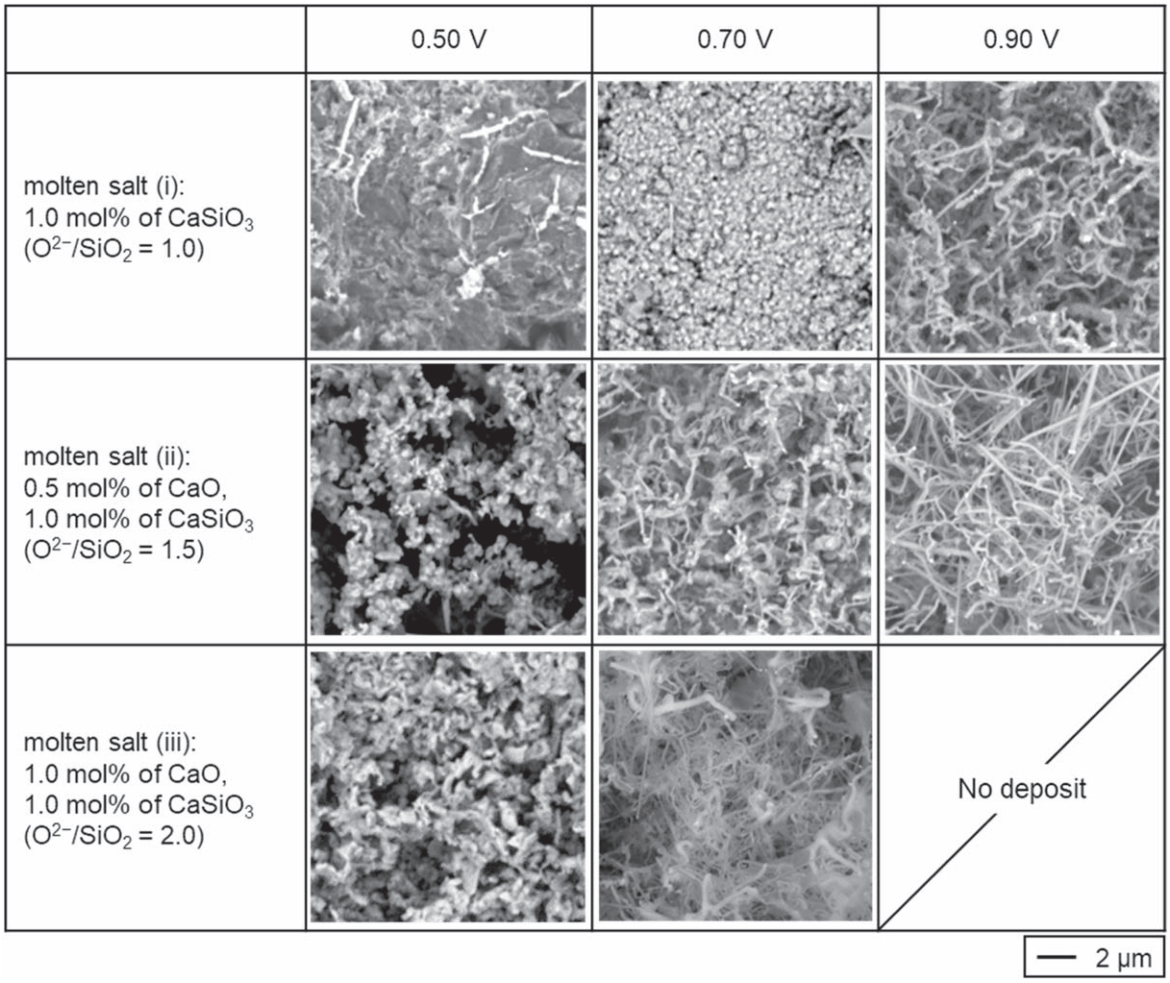

Figure 8. SEM images of the samples obtained by electrolysis (0.50 V, 0.70 V, and 0.90 V) at graphite plates in molten NaCl–$CaCl_2$ containing different amounts of CaO and $CaSiO_3$ (left vertical colum) at 1023 K. Charge density: -14 C cm^{-2}.

Nernst equation for 4-electron reaction, the difference in the reduction potential of $CaSiO_3(s)$ and $Ca_2SiO_4(s)$ was calculated to be 0.16 V, which is approximately consistent with the results of the voltammetry. As the mixture of Si and $CaSi_2$ was detected at 0.50 V, the cathodic current peak at 0.50 V is attributed to the formation of $CaSi_2$ expressed in reactions 7 and 8.

For samples obtained in molten salt (iii), the existence of pure Si was confirmed at only 0.70 V and the mixture of Si and $CaSi_2$ at 0.50 V. As only graphite was detected at 0.90 V, the increase in cathodic current from 0.75 V would correspond to the electrochemical reduction of dominant SiO_4^{4-} to solid Si (reaction 9), and the current peak at around 0.5 V is the formation of $CaSi_2$ (reaction 7, 8). The identified phases are summarized in Table II.

Figure 8 shows the surface SEM images of the deposits. In molten salt (i), wire-like Si, particle Si and dense $CaSi_2$ were obtained at 0.90, 0.70 V and 0.50 V, respectively. In molten salt (ii), wire-like Si with different shapes were deposited at 0.70 and 0.90 V, and particle Si was formed at 0.50 V. For samples obtained in molten salt (iii), wire-like Si was observed at 0.70 V and particle Si at 0.50 V. The change in morphology of reduced Si is likely due to the change of overpotential and current density. Generally, when the overpotential is low and current density low, electrodeposits become field-oriented isolated crystals type, such as wires.[45] On the other hand, when the overpotential is higher and current density higher, the electrodeposits shift to unoriented dispersion type, such as particles.[45] In molten salt (i), the potential of 0.90 V would correspond to the low overpotential and current density, which results in the formation of wire-like Si. The potential of 0.70 V is considered to be classified as the high overpotential and current density, resulting in the formation of particle Si. In molten salt (iii), the electrochemical reduction of SiO_4^{4-} starts from a more negative potential compared with SiO_3^{2-}. Then, the potential of 0.70 V corresponds to the low overpotential and current density, giving wire-like Si. The potential of 0.50 V is classified as the high overpotential and current density, resulting in the formation of particle Si. In molten salt (ii), SiO_4^{4-} and SiO_3^{2-} are dominant and second dominant species, respectively. Therefore, by the same logic as above, wire-like Si is formed from SiO_3^{2-} at 0.90 V and from SiO_4^{4-} at 0.70 V. In the same manner, particle Si is electrodeposited from SiO_4^{4-} at 0.50 V.

All the results shown above indicate that the electrodeposition of Si starts from approximately 0.2 V more positive for SiO_3^{2-} compared with SiO_4^{4-}. Considering that the formation of Ca–Zn, which reduces the current efficiency of Si–Zn alloy production, has been confirmed to proceed from 0.40 V, SiO_3^{2-}, which has a wider potential range to Ca-Zn alloy formation than SiO_4^{4-}, is more suitable for the Si–Zn alloy production. Therefore, molten salt (i), in which SiO_3^{2-} is dominant and molten salt (ii), which contains SiO_3^{2-} as a secondary dominant species, are suitable for the electrodeposition of Si at a liquid Zn cathode.

Conclusions

The ionic species and electrochemical reduction of silicate ions at a solid graphite substrate in molten eutectic NaCl–$CaCl_2$ at 1023 K with various concentrations of O^{2-} were conducted as a preliminary

study for a liquid Zn cathode. The ionic species of silicates in molten salts containing (i) 1.0 mol% $CaSiO_3$ ($r_{O^{2-}/SiO_2} = 1.0$), (ii) 0.5 mol% CaO and 1.0 mol% $CaSiO_3$ ($r_{O^{2-}/SiO_2} = 1.5$), and (iii) 1.0 mol% CaO and 1.0 mol% $CaSiO_3$ ($r_{O^{2-}/SiO_2} = 2.0$) was investigated by Raman spectroscopy. The dominant silicon ion is attributed to SiO_3^{2-} ion in molten salt (i) and SiO_4^{4-} ion in molten salt (iii), which is consistent with the r_{O^{2-}/SiO_2} in the melt. In molten salt (ii), the primary dominant species was detected as SiO_4^{4-} and secondary dominant species as SiO_3^{2-} due to the poor stability of $Si_2O_7^{6-}$. In molten salt (i), electrodeposition of Si from 1.0 V was confirmed. In molten salt (ii), electrochemical reduction of SiO_3^{2-} was indicated at 0.95 V and SiO_4^{4-} from 0.80 V. Electrochemical reduction of SiO_4^{4-} was indicated from 0.80 V in molten salt (iii). Formation of $CaSi_2$ was confirmed at 0.50 V in all molten salts and no significant differences were observed in the potential range for pure Si deposition in molten salts with $r_{O^{2-}/SiO_2} = 1.0$ and 1.5 are almost same.

Acknowledgments

This study was partially supported by Grant-in-Aid for Scientific Research A, Grant Number 16H02410, from the Japan Society for the Promotion of Science (JSPS); and The Joint Usage/Research Center for Zero Emission Energy Research (ZE2020B-58), Institute of Advanced Energy, Kyoto University.

ORCID

Takayuki Yamamoto https://orcid.org/0000-0003-3553-3272
Kouji Yasuda https://orcid.org/0000-0001-5656-5359
Toshiyuki Nohira https://orcid.org/0000-0002-4053-554X

References

1. Key World Energy Statistics 2019, *IEA*, (2019).
2. Energy Outlook 2018, *IEA* (2018).
3. Industrial Rare Metal 2019, *Arumu Publ. Co.* (2019).
4. Photovoltaic Market 2019, *RTS Corp.* (2019).
5. H. Schweickert, K. Reusche, and H. Gustsche, *U.S. Patent*, 3011877 (1961).
6. H. Gutsche, *U.S. Patent*, 3011877 (1962).
7. C. Bye and B. Ceccaroli, *Sol. Energ. Mater. Sol. C.*, **130**, 634 (2014).
8. F. Chigondo, *Silicon*, **10**, 789 (2018).
9. K. Hanazawa, N. Yuge, and Y. Kato, *Mater. Trans.*, **45**, 844 (2004).
10. G. Burns, J. Rabe, and S. Yilmaz, *PCT International Patent*, WO2005/061383 (2005).
11. K. Tang, S. Andersson, E. Nordstrand, and M. Tangstad, *JOM*, **64**, 952 (2012).
12. X. Ma, T. Yoshikawa, and K. Morita, *Sep. Purif. Technol.*, **125**, 264 (2014).
13. Y. Wang, X. Ma, and K. Morita, *Metall. Mater. Trans. B*, **45**, 334 (2014).
14. T. Shimamune and I. Yoshikawa, *Japanese Patent Toku Kai*, H15–342016 (2003).
15. E. Robert and T. Zijlema, *PCT International Patent*, WO2006/100114 (2006).
16. S. Sakaguchi, *PCT International Patent*, WO2007/119605 (2007).
17. S. Honda, M. Yasueda, S. Hayashida, and M. Yamaguchi, *Japanese Patent Toku Kai*, H19–145663 (2007).
18. T. Nohira, K. Yasuda, and Y. Ito, *Nat. Mater.*, **2**, 397 (2003).
19. K. Yasuda, T. Nohira, and Y. Ito, *J. Phys. Chem. Solids*, **66**, 443 (2005).
20. K. Yasuda, T. Nohira, K. Takahashi, R. Hagiwara, and Y. H. Ogata, *J. Electrochem. Soc.*, **152**, D232 (2005).
21. K. Yasuda, T. Nohira, K. Amezawa, Y. H. Ogata, and Y. Ito, *J. Electrochem. Soc.*, **152**, D69 (2005).
22. K. Yasuda, T. Nohira, R. Hagiwara, and Y. H. Ogata, *Electrochim. Acta*, **53**, 106 (2007).
23. K. Yasuda, T. Nohira, R. Hagiwara, and Y. H. Ogata, *J. Electrochem. Soc.*, **154**, E95 (2007).
24. Y. Nishimura, T. Nohira, K. Kobayashi, and R. Hagiwara, *J. Electrochem. Soc.*, **158**, E55 (2011).
25. T. Toba, K. Yasuda, T. Nohira, X. Yang, R. Hagiwara, K. Ichitsubo, K. Masuda, and T. Homma, *Electrochemistry*, **81**, 559 (2013).
26. X. Yang, K. Yasuda, T. Nohira, R. Hagiwara, and T. Homma, *Metall. Mater. Trans. B*, **45**, 1337 (2014).
27. X. Yang, K. Yasuda, T. Nohira, R. Hagiwara, and T. Homma, *J. Electrochem. Soc.*, **161**, D3116 (2014).
28. X. Yang, K. Yasuda, T. Nohira, R. Hagiwara, and T. Homma, *Metall. Mater. Trans. B*, **47**, 788 (2015).
29. X. Yang, K. Yasuda, T. Nohira, R. Hagiwara, and T. Homma, *Metall. Mater. Trans. E*, **3**, 145 (2016).
30. M. Zhong, K. Yasuda, T. Homma, and T. Nohira, *Electrochemistry*, **86**, 77 (2018).
31. M. Zhong, X. Yang, K. Yasuda, T. Homma, and T. Nohira, *Metall. Mater. Trans. B*, **49B**, 341 (2018).
32. T. Nohira, A. Ido, T. Shimao, X. Yang, K. Yasuda, R. Hagiwara, and T. Homma, *ECS Trans.*, **75**, 17 (2016).
33. K. Yasuda, T. Shimao, R. Hagiwara, T. Homma, and T. Nohira, *J. Electrochem. Soc.*, **164**, H5049 (2017).
34. Y. Ma, A. Ido, K. Yasuda, R. Hagiwara, and T. Nohira, *J. Electrochem. Soc.*, **166**, D162 (2019).
35. X. Yang, L. Ji, X. Zou, T. Lim, J. Zhao, E. T. Yu, and A. J. Bard, *Angew. Chem. Int. Ed.*, **56**, 15078 (2017).
36. X. Zou, L. Ji, X. Yang, T. Lim, E. T. Yu, and A. J. Bard, *J. Am. Chem. Soc.*, **139**, 16060 (2017).
37. X. Zou, L. Ji, J. Ge, D. R. Sadoway, E. T. Yu, and A. J. Bard, *Nat. Commun.*, **10**, 5772 (2019).
38. S. Wang, F. Zhang, X. Liu, and L. Zhang, *Thermochim. Acta*, **470**, 105 (2008).
39. B. O. Mysen, D. Virgo, and C. M. Scarfe, *Am. Mineral.*, **65**, 690 (1980).
40. D. Virgo, B. O. Mysen, and I. Kushiro, *Science*, **208**, 1371 (1980).
41. B. O. Mysen, *Structure and Properties of Silicate Melts* (Elsevier, Amsterdam) (1988).
42. C. Wang, J. Zhang, Z. Liu, K. Jiao, G. Wang, J. Yang, and K. Chou, *Metall. Mater. Trans. B*, **48**, 328 (2017).
43. L. B. Pankratz, *Thermodynamic Properties of Carbides, Nitrides, and Other Selected Substances* (U. S. Bureau of Mines (USBM))(Washington D.C.) (1994).
44. M. W. Chase, *NIST-JANAF Thermochemical Tables, 4th ed., Part I Al-Co* (American Chemical Society, and the American Institute of Physics for the National Institute of Standards and Technology, New York, NY) (1998).
45. R. Winand, *Electrochim. Acta*, **39**, 1091 (1994).